BLOOD FLOW ANALYSIS USING VOXEL INFORMATION

Nami MATSUNAGA*, Hao LIU** and Ryutaro HIMENO***

* Computer and Information Division, Advanced Computing Center, RIKEN
2-1 Hirosawa, Wako, Saitama 351-0198, Japan
E-mail: matunaga@postman.riken.go.jp
** Computer and Information Division, Advanced Computing Center, RIKEN
2-1 Hirosawa, Wako, Saitama 351-0198, Japan
E-mail: hliu@postman.riken.go.jp
*** Computer and Information Division, Advanced Computing Center, RIKEN
2-1 Hirosawa, Wako, Saitama 351-0198, Japan
E-mail: himeno@postman.riken.go.jp

Abstract. *A blood flow analysis based on the medical image data obtained by magnetic-resonance imaging (MRI) and computed tomography (CT) is usually done by the finite element method or finite volume method in a boundary-fitted coordinate (BFC) system. However, considerable time and effort is sometimes necessary to make a model of the blood vessels from the actual image data. We propose a new computational fluid dynamic method in this paper to solve the time and effort problem. We paid attention to the orthogonality of the pixel or voxel data obtained from the image information, and directly translated the image data into the Cartesian coordinate system by using the fractional volume of fluid (VOF) method. The flow was computed by using a non-staggered finite difference method, in which the boundary conditions were treated by the neighboring point local collocation (NPLC) method. We produced numerical results for the flow in a two-dimensional stenosed blood vessel model. A comparison with other reliable results shows that the proposed method can reasonably predict the complicated vortical flow in a blood vessel. The numerical result for the blood vessel model with a moving boundary is also presented.*

1. Introduction

The blood vessels in the circulatory system create variations in the blood flow because the system has a very complex geometrical structure, for example, sharp curvature, torsion, stenosis and aneurysm. Moreover the variation in this flow is made more unstable and complicated due to the characteristic beating, and the blood vessels may consequently be exposed to strong shear stress by this influence. These haemodynamic characteristics make it difficult to understand the detailed flow fields with application to wall shear stress (WSS), a major factor in the onset, development and outcome of arteriosclerosis (Fry et al. [1], Caro [2], Ku et al. [3]). However, it is very important to check the geometrical vascular influence for clinical purposes. We propose in this paper a new method which makes use of the orthogonality of image data (pixel and voxel information) originating from magnetic-resonance imaging (MRI) and computed tomography (CT) as a method to achieve this. The boundaries of the object can be

described by the fractional volume of fluid (VOF) method introduced by Hirt et al. [4] that is defined from the color information of each pixel or voxel obtained from the image. The computational domain can then be discretized simply in the Cartesian coordinate system. The pressure conditions at the boundary stencils are defined by using the Neumann conditions combined with the governing equations. The flow is computed by using the non-staggered finite difference method of Nishida [5], in which the boundary conditions are treated by the neighboring point local collocation (NPLC) method of Nakano et al. [6, 7].

A detailed description of the method is next given, and the results of two pulsatile flows in a two-dimensional stenosed blood vessel model are presented. A comparison with the reliable results of Liu et al. [8, 9] will show that the present method can reasonably predict the complicated vortical flow in a blood vessel. The numerical result for the flow in a blood vessel with a moving boundary is presented as the application.

2. Definition of the geometric model and incoming flow

Consider the following two-dimensional stenosed channel model [8, 9, 10] depicted in Fig. 1.

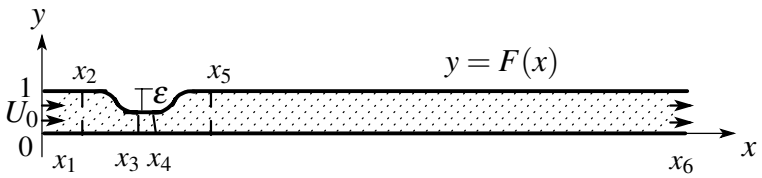

Fig. 1 Computational stenosis model

The upper wall can be described by the following functions:

$$\begin{aligned}
&F(x) = 1 && (x_1 < x < x_2),\\
&F(x) = 1 - 0.5\varepsilon\{1 + \tanh\alpha(x - x_a)\} && (x_2 \le x \le x_3),\\
&F(x) = 1 - \varepsilon && (x_3 < x < x_4),\\
&F(x) = 1 - 0.5\varepsilon\{1 - \tanh\alpha(x - x_b)\} && (x_4 \le x \le x_5),\\
&F(x) = 1 && (x_5 < x < x_6),
\end{aligned}$$

where

$$x_a = (x_2 + x_3)/2 \ \text{ and } \ x_b = (x_4 + x_5)/2,$$

α is the slope parameter, x_i $(i = 1, \ldots, 6)$ are constants, and ε is the height of the stenoses. We set $\alpha = 4.14$, and $0.1 \le \varepsilon \le 0.6$. At inlet, the waveforms of two pulsatile flows with a mean velocity of U_0 as shown in Fig. 1 are defined as follows:

$$U_0(t) = \begin{cases} 0.5(1 - \cos(2\pi t)) & \text{(Sinusoidal)},\\ 0.251 + 0.290(\cos\varphi + 0.97\cos 2\varphi + 0.47\cos 3\varphi + 0.14\cos 4\varphi) & \\ & \text{(Non-sinusoidal)}, \end{cases}$$

where $\varphi = 2\pi t - 0.14142$. Points a, b, c, d, e and f in Fig. 2 denote the points where $\partial U_0/\partial t$ and $\partial^2 U_0/\partial t^2 = 0$.

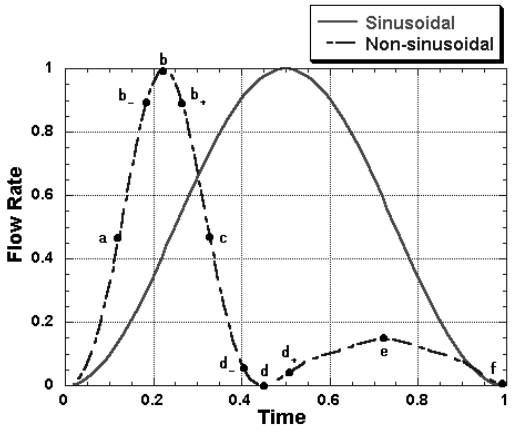

Fig. 2 Graph of incoming flows

3. Determination of the boundary from voxel information

The color information of each voxel based on MRI images can be described by voxel data as the fractional volume of fluid (VOF), where V varies over the range of $0 \leq V \leq 1$. The value V is regarded as the volume of fluid in each voxel, which implies that a boundary exists inside the voxel with a value of $0 < V < 1$. We next decide the boundary of a given domain.

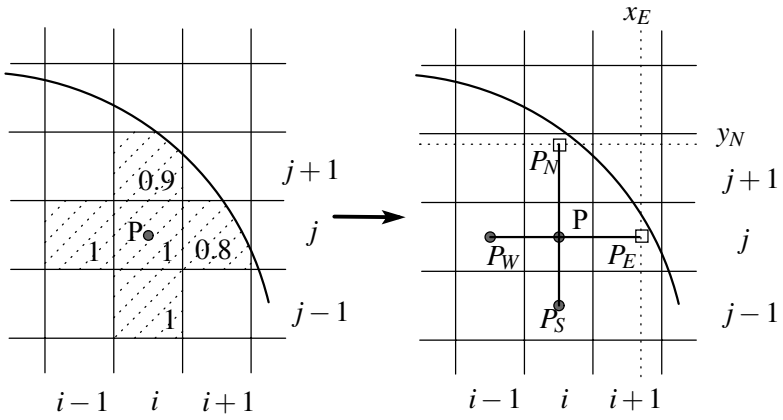

Fig. 3 Transformation

First, suppose that rectangular domain Ω covering stenosed model Ω_1 is given, and the voxel data are defined with a grid spacing of $h = \Delta x$ and $k = \Delta y$ in the x and y directions for Ω, respectively. Grid points are basically located at the center of each voxel or cell. The four grid points of the cell denoted by P_E, P_W, P_S and P_N are adjacent to $P \in \Omega_1$, and their distances from P are denoted by h_E, h_W, k_S and k_N (cf. Fig. 3). If $V(P_{ij}) = 1$ and $V(P_{i+1,j}) \neq 1$, the spatial coordinates of the point P_E corresponding to one of the boundary points illustrated in Fig. 3 are defined such that

$$(x_E, y_E) = (ih + h_E, jk),$$

where $h_E = (0.5 + V(P_E))h$.

4. Numerical methods

The two-dimensional, non-steady, incompressible Navier-Stokes equations are written as

$$\frac{\partial u}{\partial t}St = F_u - \frac{\partial p}{\partial x}, \quad \frac{\partial v}{\partial t}St = F_v - \frac{\partial p}{\partial y}, \tag{1}$$

$$D := \frac{\partial u}{\partial x} + \frac{\partial v}{\partial y} = 0, \tag{2}$$

where (u, v) are velocity components, p is the pressure, St is the Strouhal number, and F_u and F_v are flux terms defined as

$$F_u := -u\frac{\partial u}{\partial x} - v\frac{\partial u}{\partial y} + \frac{1}{\mathrm{Re}}\left(\frac{\partial^2 u}{\partial x^2} + \frac{\partial^2 u}{\partial y^2}\right), \tag{3}$$

$$F_v := -u\frac{\partial v}{\partial x} - v\frac{\partial v}{\partial y} + \frac{1}{\mathrm{Re}}\left(\frac{\partial^2 v}{\partial x^2} + \frac{\partial^2 v}{\partial y^2}\right), \tag{4}$$

where Re is the Reynolds number. Note that the volume of fluid at each voxel should be calculated in advance. Cell-vertex architecture for the velocity (u, v) and pressure p was employed, and the non-staggered finite difference method by Nishida [5] was utilized for spatial discretization. However, since this method requires ideal points for calculating the differential terms at the boundary, the neighboring point local collocation (NPLC) method by Nakano et al. [6, 7] was introduced near the boundary. To solve Eqs. (1) and (2), we used the method of line approach which decouples spatial discretization from temporal discretization. Furthermore, since the divergence-free condition is satisfied at each time step, the coupled form of velocity and pressure was used. Details of algorithm are given next.

- **Algorithm**

Step 1. Time integration is discretized by using the Adams-Bashforth method with secondary accuracy for the flux terms, and the explicit Euler method is employed for the other terms. The transient velocity (u^*, v^*) at time step $n+1$ can be expresssed as

$$u^*_{i+\frac{1}{2},j} = u^n_{i+\frac{1}{2},j} + \frac{\Delta t}{St}\left(\frac{3{F_u}^n{}_{i+\frac{1}{2},j} - {F_u}^{n-1}{}_{i+\frac{1}{2},j}}{2} - \left.\frac{\partial p^n}{\partial x}\right|_{i+\frac{1}{2},j}\right),$$

$$v^*_{i,j+\frac{1}{2}} = v^n_{i,j+\frac{1}{2}} + \frac{\Delta t}{St}\left(\frac{3{F_v}^n{}_{i,j+\frac{1}{2}} - {F_v}^{n-1}{}_{i,j+\frac{1}{2}}}{2} - \left.\frac{\partial p^n}{\partial y}\right|_{i,j+\frac{1}{2}}\right),$$

where superscript n denotes the nth time step, Δt is the time step, and i and j are grid points in the x and y derections, respectively. We set ${F_u^0}_{i+1/2,j} := {F_u^1}_{i+1/2,j}$ and ${F_v^0}_{i,j+1/2} := {F_v^1}_{i,j+1/2}$.

Step 2. To compute pressure p^{n+1}, we can write

$$u^{n+1}_{i+\frac{1}{2},j} - u^*_{i+\frac{1}{2},j} = \frac{\Delta t}{St}\left(-\left.\frac{\partial p^{n+1}}{\partial x}\right|_{i+\frac{1}{2},j} + \left.\frac{\partial p^n}{\partial x}\right|_{i+\frac{1}{2},j}\right), \tag{5}$$

$$v_{i,j+\frac{1}{2}}^{n+1} - v_{i,j+\frac{1}{2}}^{*} = \frac{\Delta t}{St}\left(-\frac{\partial p^{n+1}}{\partial y}\Big|_{i,j+\frac{1}{2}} + \frac{\partial p^{n}}{\partial y}\Big|_{i,j+\frac{1}{2}}\right) \tag{6}$$

and

$$D_{i,j}^{n+1} = 0. \tag{7}$$

Substituing Eqs. (5) and (6) into Eq. (7), a pressure-based Poisson equation results such that

$$\frac{\partial^2 p^{n+1}}{\partial x^2}\Big|_{i,j} + \frac{\partial^2 p^{n+1}}{\partial y^2}\Big|_{i,j} = \frac{St}{\Delta t} D_{i,j}^{*} + \frac{\partial^2 p^{n}}{\partial x^2}\Big|_{i,j} + \frac{\partial^2 p^{n}}{\partial y^2}\Big|_{i,j}.$$

Step 3. We can calculate from Eqs. (5) and (6) the velocity at a time step. If $|D_{i,j}^{n+1}| < \varepsilon^*$, where ε^* is a small constant, this can be updated as

$$u_{i+\frac{1}{2},j}^{*} = u_{i+\frac{1}{2},j}^{n+1}, \quad v_{i,j+\frac{1}{2}}^{*} = v_{i,j+\frac{1}{2}}^{n+1}, \quad p_{i,j}^{n} = p_{i,j}^{n+1}$$

before returning to Step 2. Otherwise, go back to Step 1.

Note that the flux terms at the mid-point of each cell side need to be calculated in Step 1. In order to calculate these terms, the non-staggered finite difference method of Nishida [5] was used. The velocity at each cell center can be calculated by using the mean value of two adjacent grid points as follows:

$$u_{i\pm\frac{1}{2},j} = \frac{u_{i,j} + u_{i\pm1,j}}{2}, \qquad v_{i,j\pm\frac{1}{2}} = \frac{v_{i,j} + v_{i,j\pm1}}{2}. \tag{8}$$

Hence, we have

$$\begin{aligned}
\frac{\partial^2 u}{\partial x^2}\Big|_{i+\frac{1}{2},j} &= \frac{1}{2h}\left(\frac{u_{i+2,j} - u_{i+1,j}}{h} - \frac{u_{i,j} - u_{i-1,j}}{h}\right), \\
\frac{\partial^2 u}{\partial y^2}\Big|_{i+\frac{1}{2},j} &= \frac{1}{2}\left(\frac{u_{i+1,j} - 2u_{i+1,j} + u_{i+1,j-1}}{k^2} + \frac{u_{i,j} - 2u_{i,j} + u_{i,j-1}}{k^2}\right)
\end{aligned} \tag{9}$$

for the discretization of flux term $F_{ui+1/2,j}$. Similarly, we can also calculate the viscous term of $F_{vi,j+1/2}$.

The differential terms at neighboring points $(i+1/2, j)$ and $(i, j+1/2)$ on the boundary can be calculated by using the neighboring point local collocation (NPLC) method [6, 7] in terms of the flux to avoid the use of ideal points. With the local collocation method, the two-dimensional spatial derivatives at the boundary stencils are approximated as follows.

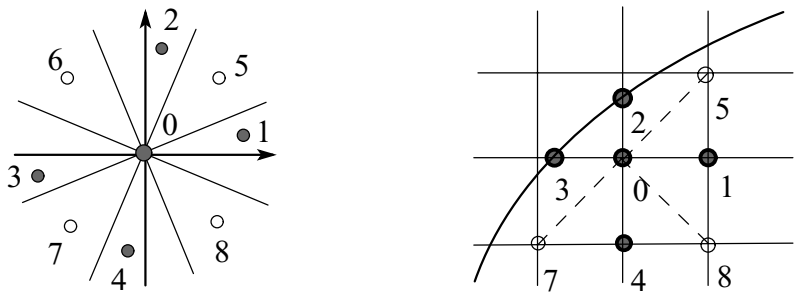

Fig. 4 Spacial point relationship for NPLC

We first numbered the points as shown in Fig. 4 and assumed that the flow variable can be approximated by

$$f(x,y) = f_0 + a_1 x + a_2 y + a_3 x^2 + a_4 y^2 + a_5 xy, \tag{10}$$

where f_0 represents the value at the current point, a_i $(i = 1,\ldots,5)$ are unknown coefficients, and (x,y) are the relative coordinates from the current point. Note that we can obtain the following spatial derivatives at point 0 shown in Fig. 4:

$$\frac{\partial f}{\partial x} = a_1 + 2a_3 x + a_5 y, \qquad \frac{\partial f}{\partial y} = a_2 + 2a_4 y + a_5 x,$$
$$\frac{\partial^2 f}{\partial x^2} = 2a_3, \qquad \frac{\partial^2 f}{\partial y^2} = 2a_4$$

by differentiating Eq. (10) with respect to x or y. To get unknown coefficients a_i $(i = 1,\ldots,5)$, the following matrices for $l = 5,\ldots,8$ are solved and averaged to ensure the spatial second-order accuracy:

$$\begin{pmatrix} x_1 & y_1 & x_1^2 & y_1^2 & x_1y_1 \\ x_2 & y_2 & x_2^2 & y_2^2 & x_2y_2 \\ x_3 & y_3 & x_3^2 & y_3^2 & x_3y_3 \\ x_4 & y_4 & x_4^2 & y_4^2 & x_4y_4 \\ x_l & y_l & x_l^2 & y_l^2 & x_ly_l \end{pmatrix} \begin{pmatrix} a_1 \\ a_2 \\ a_3 \\ a_4 \\ a_5 \end{pmatrix} = \begin{pmatrix} f_1 - f_0 \\ f_2 - f_0 \\ f_3 - f_0 \\ f_4 - f_0 \\ f_l - f_0 \end{pmatrix} \qquad (l = 5,\ldots,8).$$

If a grid point in the diagonal direction (for example, point 6 in Fig. 4) is not in region Ω_1, the calculation of the matrix is skipped.

We use for the convection terms the third-order upwind scheme at the usual inner grids and an alternative upwind scheme of first-order by the NPLC method at the boundary. Note that we further introduce the following method to assess the convection terms at points $(i+1/2, j)$ and $(i, j+1/2)$. For example, $u \cdot \partial u/\partial x$, one of the convection terms in F_u at point $P_{i+1/2,j}$ is calculated by the third-order upwind scheme such as

$$u\frac{\partial u}{\partial x}\Big|_{i+\frac{1}{2},j} \approx \begin{cases} u_{i+\frac{1}{2},j} \cdot \dfrac{2d_{1+} + 3d_0 - 6d_{1-} + d_{2-}}{6h} & u_{i+\frac{1}{2},j} > 0, \\ u_{i+\frac{1}{2},j} \cdot \dfrac{-d_{2+} + 6d_{1+} - 3d_0 - 2d_{1-}}{6h} & u_{i+\frac{1}{2},j} \le 0, \end{cases} \tag{11}$$

where

$$d_{2-} = \frac{u_{i-2,j} + u_{i-1,j}}{2}, \qquad d_{1-} = \frac{u_{i-1,j} + u_{i,j}}{2}, \qquad d_0 = \frac{u_{i,j} + u_{i+1,j}}{2},$$
$$d_{1+} = \frac{u_{i-1,j} + u_{i+2,j}}{2}, \qquad d_{2+} = \frac{u_{i-2,j} + u_{i+3,j}}{2},$$

if all referring to grid points are included in region Ω_1. Otherwise, we calculate the terms by using the first and second differentiable terms with the NPLC method as follows:

$$u\frac{\partial u}{\partial x}\Big|_{i+\frac{1}{2},j} \approx u_{i+\frac{1}{2},j}\delta_x u_{i+\frac{1}{2},j} - \frac{|u_{i+\frac{1}{2},j}|h}{2} \cdot \delta_{xx} u_{i+\frac{1}{2},j}, \tag{12}$$

where $\delta_x u$ and $\delta_{xx} u$ are the respective values for the first and second differentiation obtained from NPLC. The convection terms in the y direction can be similarly obtained.

5. Boundary conditions

In the solutions to the Navier-Stokes equations with Dirichlet conditions, we usually need the Neumann conditions for the pressure. However, it is very difficult to treat the boundary conditions for an arbitrary region, except a square or a rectangle, in the Cartesian coordinate system. We propose a new method that is based on Eq. (1) to solve this problem.

Let $n = (n_x, n_y)$ be the unit outer normal vector. When the no-slip condition at the boundary is imposed, it holds that

$$\frac{\partial p}{\partial n} = \frac{\partial p}{\partial x} n_x + \frac{\partial p}{\partial y} n_y = 0 \tag{13}$$

for the pressure. Moreover, if $n_x \neq 0$ and $n_y \neq 0$, we can obtain

$$\frac{\partial p}{\partial x} = \frac{1}{2}\left\{ F_u - \frac{\partial u}{\partial t} St - \frac{n_y}{n_x}\left(F_v - \frac{\partial v}{\partial t} St \right) \right\} \tag{14}$$

from Eqs. (1) and (13). Therefore, if P_E is a boundary point on the right of point P_{ij}, we can calculate $p(P_E)$ by using

$$\frac{\partial p}{\partial x} \simeq \frac{p(P_E) - p(P_{ij})}{h_E},$$

where $p(P_E)$ and $p(P_{ij})$ denote the pressures at points P_E and P_{ij}, and h_E denotes the distance between P_E and P_{ij}. In the case of $n_x = 1$ and $n_y = 0$, we can use

$$\frac{\partial p}{\partial x} = F_u - \frac{\partial u}{\partial t} \cdot St.$$

6. Numerical results

Computations were conducted for $\mathrm{Re} = 750$ and $St = 0.024$ with a stenosed channel of $\varepsilon = 0.5$. We set $x_1 = 0,\ x_2 = 5.0,\ x_3 = x_4 = 7.5,\ x_5 = 10.0$ and $x_6 = 28.0$. A grid system with a uniform grid spacing of $h = k = 0.05$ was used for all the cases in this section. The time step was set to $\Delta t = 1.25 \times 10^{-4}$, and the computations were carried out up to 8000 steps. At the solid wall of the channel, we apply the following non-slip condition for the velocity components:

$$(u, v) = (0, 0).$$

The inflow conditions are taken as

$$(u, v) = (U_0, 0).$$

For the outgoing flow conditions, we use

$$\frac{\partial u}{\partial x} = 0, \quad \frac{\partial v}{\partial x} = 0, \quad \frac{\partial U_0}{\partial t} St = -\frac{\partial p}{\partial x}.$$

The initial condition is that the flow is at rest at $t = 0$. The poisson equation for the pressure is solved by using the SOR method with acceleration parameter $\omega = 1$. The wall shear stress (WSS; τ_w) is defined as the dimensionless shear stress on the wall surface such that $\tau_w = (\partial u/\partial y)_{\mathrm{wall}}/\mathrm{Re}$.

The WSS distributions on the lower walls are plotted in Figs. 5–6. Figures 7–8 show iso-velocity and pressure contours for the non-sinusoidal cases. Figures 5–6 show that a higher stress occurred immediately behind the stenosed portion when the pulsatile flow was just over the peak in both cases. Moreover, as shown in Figs. 7–8, when the flow decelerated, the wavy core flow behind the stenoses gradually developed strong vortices as detected by Liu et al. Since the inflow velocity changed rapidly in the case of the non-sinusoidal waveform, the vortices were stronger than in the case of sinusoidal waveform. Overall, we believe the vortex wave flow is dominated not only by the stenoses geometry, but also by the waveform of the inflow.

7. Application to a blood vessel with a moving boundary

This example is treated by the following blood vessel a model with a moving boundary (cf. Ralph [11] and Liu et al. [12]). The upper wall is defined by the following function:

$$H(x,t) = 1 - F(x)T(t)$$

where $F(x)$ is the function defined in section 2 and $T(t) = 0.5(1-\cos 2\pi t)$.

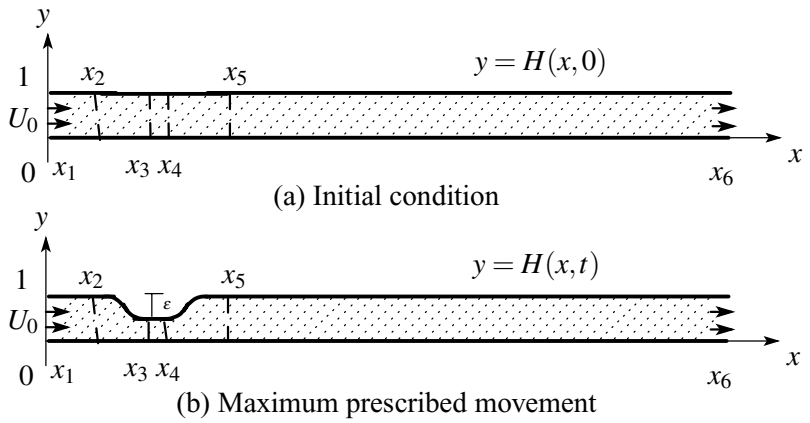

Fig. 9 Computational stenosis models

Let U_0 be Poiseuille flow. We put $x_1 = 0.0$, $x_2 = 3.0$, $x_3 = 5.5$, $x_4 = 13.5$, $x_5 = 16.0$ and $x_6 = 28.0$. We use voxel data which are calculated for each time step. Although the algorithm in section 4 is used, care must be taken when handling values (u^*, v^*) and p^n at the points near the boundary; that is, interpolation should be necessary.

As the boundary conditions, the non-slip condition $(u,v) = (0, St \cdot \partial H(x,t)/\partial t)$ is used for the velocity components at the upper wall surface. The velocity gradient at outlet is fixed to zero as $\partial u/\partial x = \partial v/\partial x = 0$. We use $(u,v) = (U_0, 0)$ as the initial condition at $t = 0$.

The numerical results for the blood vessel model with the parameters $\mathrm{Re} = 300$, $St = 0.057$ and $\varepsilon = 0.4$ which was treated by Liu et al. [12] are shown in Figs. 10–11. The mesh sizes and time step length were $h = k = 0.05$ and $\Delta t = 0.0002$, respectively. Computation was carried out up to 5000 steps. As Figs. 10–11 indicate, it was possible to perform a blood flow analysis for the blood vessel model with a moving boundary, even if the Cartesian coordinate system was used.

8. Conclusions

The results of the present study demonstrate the feasibility of medical image-based computational fluid dynamic modeling of complex pulsatile, vortical blood flow directly in a Cartesian coordinate system. This method shows great potential for definition of the boundary based on voxel information, as well as for grid generation in the case of complex geometry. A quantitative comparison with other reliable results confirms that our method can reasonably predict not only a vortical flow pattern, but also a wall shear stress distribution. The application to simulating the blood flow in a caritod artery based on MR images is currently underway, and an extension to the three-dimensional case is also under consideration.

References

[1] D. L. Fry, Localizing factors in arteriosclerosis, in *Atherosclerosis and Coronary Heart Disease*, ed. by W. Likoff, B. L. Segal, W. Insull, Jr., Grune and Stratton (1972), 85-104.

[2] C. G. Caro, J. M. Fitz-gerald, and R. C. Schroter, Atheroma and arterial wall shear: observation, correlation and proposal of a shear dependent mass transfer mechanism for atherogenesis, *Proc. Royal Society London*, B177 (1971), 109-159.

[3] D. N. Ku, D. P. Giddens, C. K. Zarins, and S. Glagov, Pulsatile flow and atherosclerosis in the human carotid bifurcation: Positive correlation between plaque location and low and oscillating shear stress, *Arteriosclerosis*, Vol. 5 (1985), 541–567.

[4] C. W. Hirt, and B. D. Nichols, Volume of fluid (VOF) method for the dynamics of free boundaries, *J. Comp. Phys.*, 39 (1981), 201–225.

[5] H. Nishida, Numerical solutions of incompressible Navier-Stokes equations using non-staggered finite difference methods, *JSME*, B-62-599 (1996), 2646–2651 (in Japanese).

[6] N. Satofuka, K. Morinishi, and A. Nakano, Parallel implementation of gridless algorithm for compressible flow equations, in *Parallel Computational Fluid Dynamics: New Algorithms and Applications* (ed. by N. Satofuka, J. Periaux and A. Ecer), Elsevier (1995), 349–356.

[7] A. Nakano, N. Satofuka, and N. Shimomura, A Cartesian grid approach to compressible viscous flow computations, in *Computational Fluid Dynamics '96*, John Wiley & Sons (1996), 540–546.

[8] H. Liu, and T. Yamaguchi, Effects of pulsation and geometry on post-stenotic oscillatory flow, *JSME Int. J.*, Series C, 42, No. 3 (1999), 612–620.

[9] H. Liu, and T. Yamaguchi, Waveform dependence of pulsatile flow in a stenosed channel, *ASME J. Biomech. Eng.*, 123 (2001), 88–96.

[10] O. R. Tutty, Pulsatile flow in a constricted channel, *ASME J. Biomech. Eng.*, 114 (1992), 50–54.

[11] M. E. Ralph, and T. J. Pedley, Flow in a channel with time-dependent indentation in one wall, *J. Fluid. Eng.*, 112 (1990), 468–475.

[12] H. Liu, and T. Yamaguchi, Computational fluid mechanics of the vortical flow in blood vessel, in *Clinical Application of Computational Mechanics to the Cardiovascular System* (ed. by T. Yamaguchi), Springer-Verlag Tokyo (2000), 136–156.

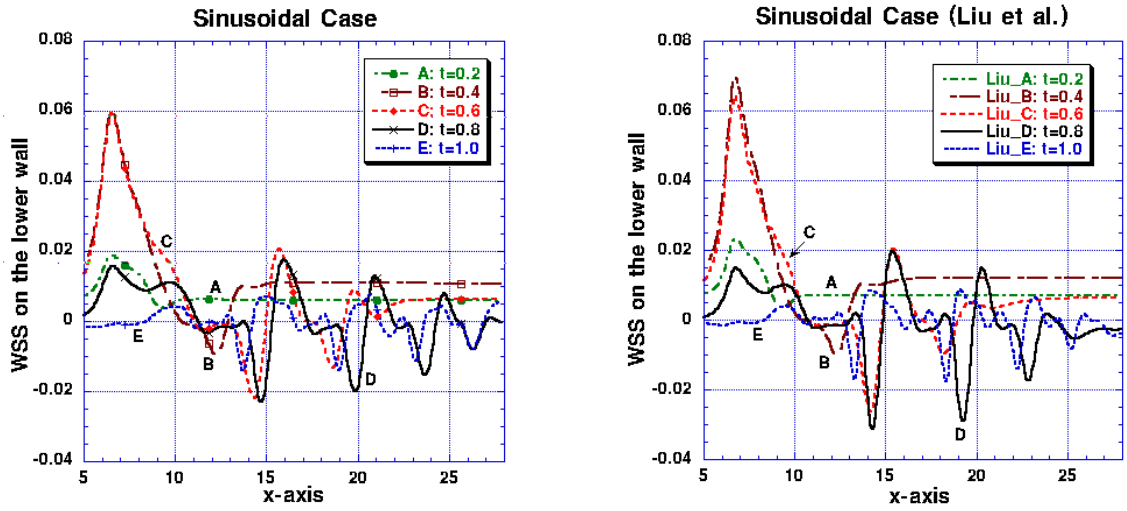

(a) Present work (b) Liu et al. (2001)

Fig. 5 WSS at Re = 750 and $St = 0.024$ with $\varepsilon = 0.5$ in the sinusoidal case

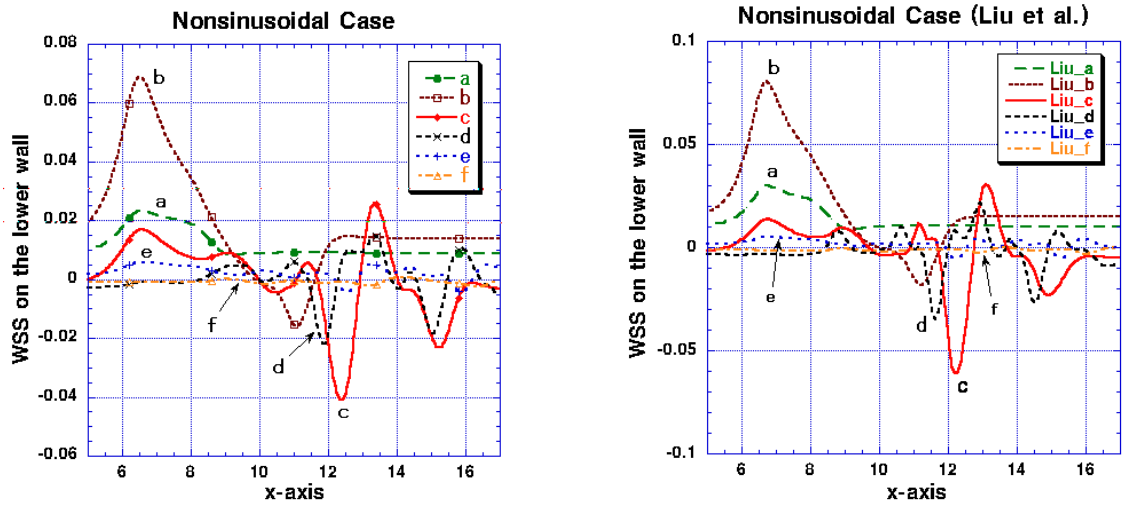

(a) Present work (b) Liu et al. (2001)

Fig. 6 WSS at Re = 750 and $St = 0.024$ with $\varepsilon = 0.5$ in the non-sinusoidal case

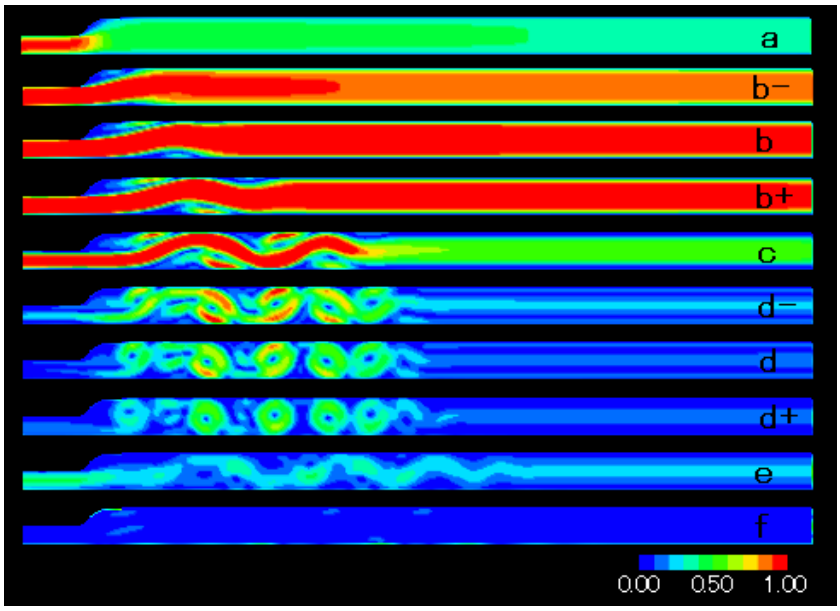

(a) Present work

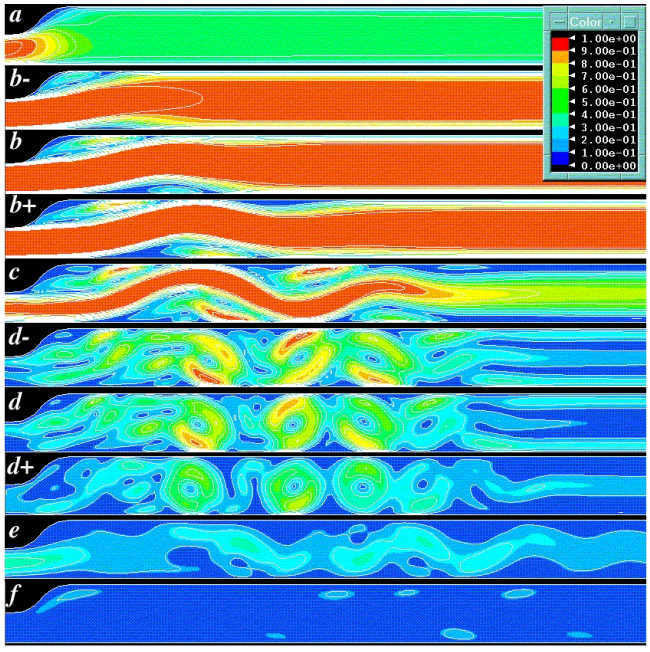

(b) Liu et al. (2001)

Fig. 7 Iso-velocity contours at Re = 750 and $St = 0.024$ with $\varepsilon = 0.5$ in the non-sinusoidal case

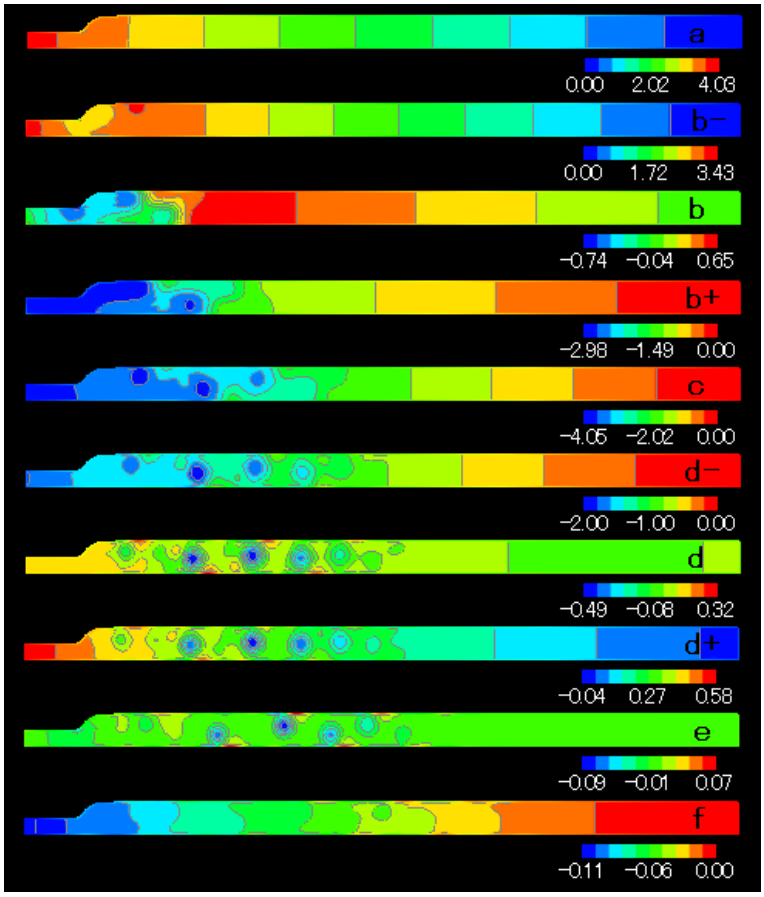

(a) Present work

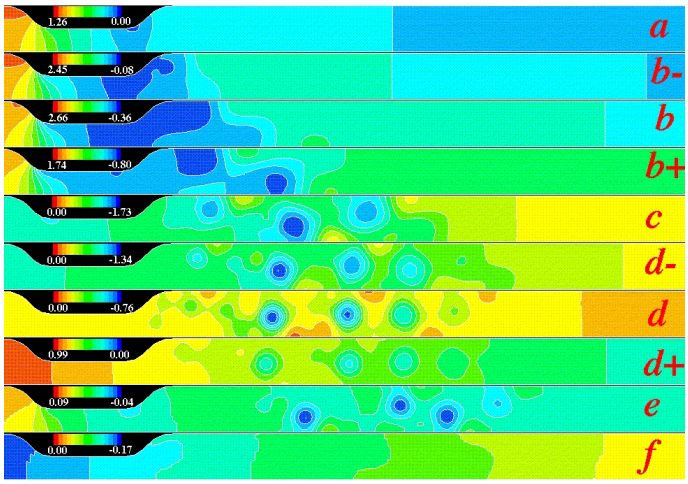

(b) Liu et al. (2001)

Fig. 8 Pressure contours at Re = 750 and $St = 0.024$ with $\varepsilon = 0.5$ in the non-sinusoidal case

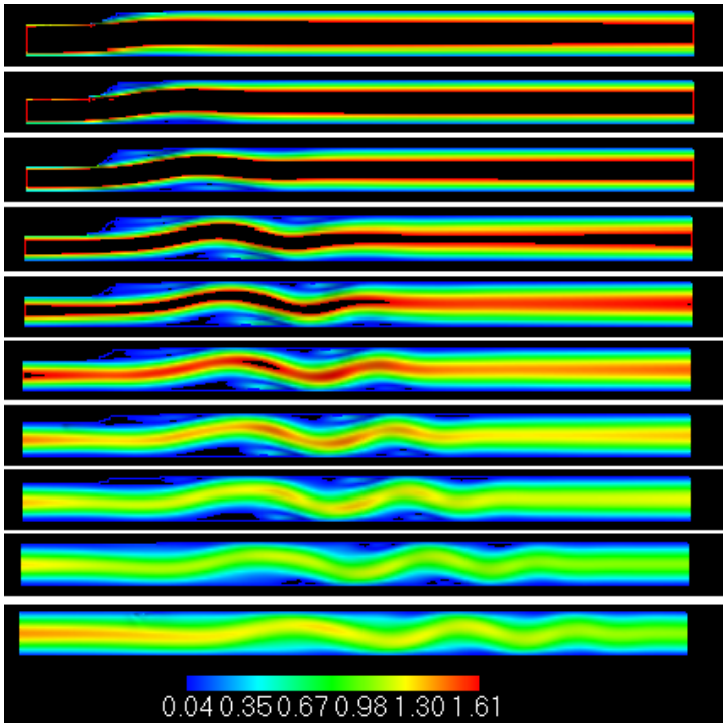

(a) Present work

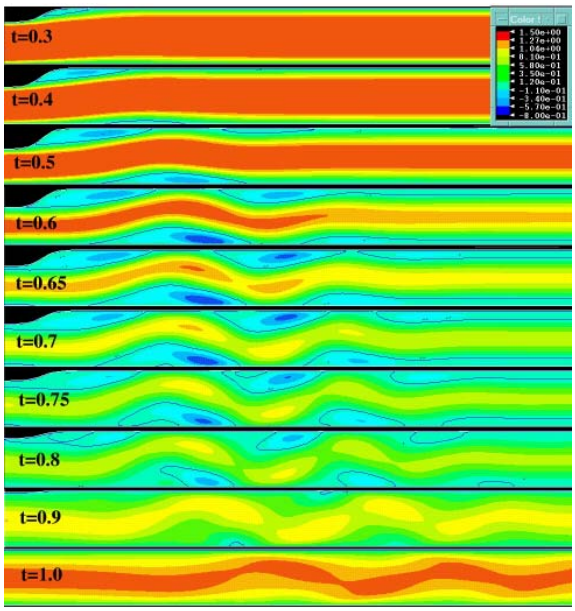

(b) Liu et al. (2000)

Fig. 10 Iso-velocity contours at Re = 300 and $St = 0.057$ with $\varepsilon = 0.4$

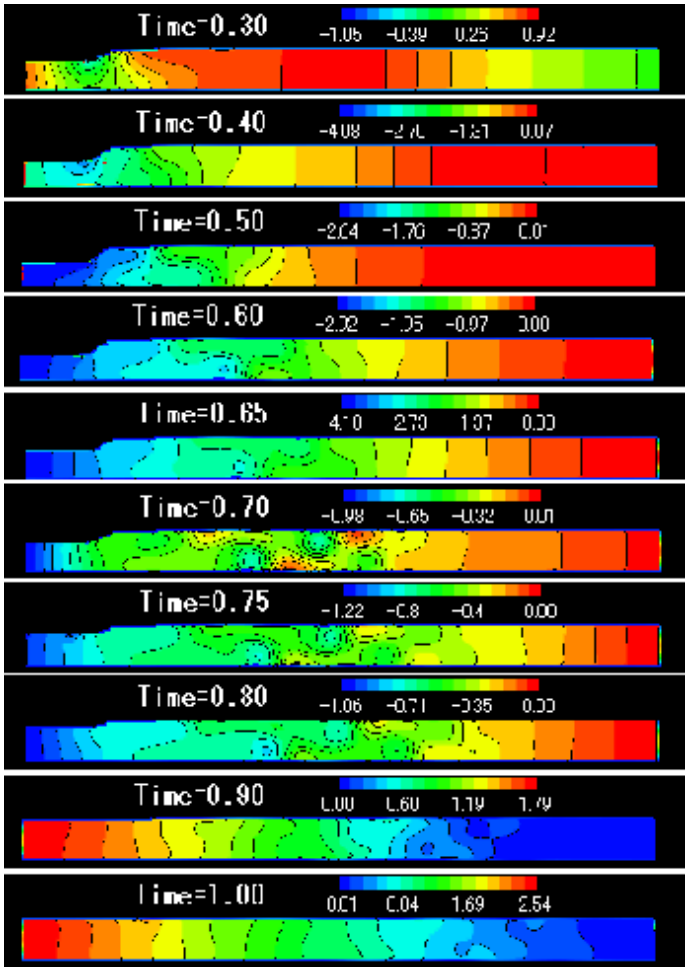

(a) Present work

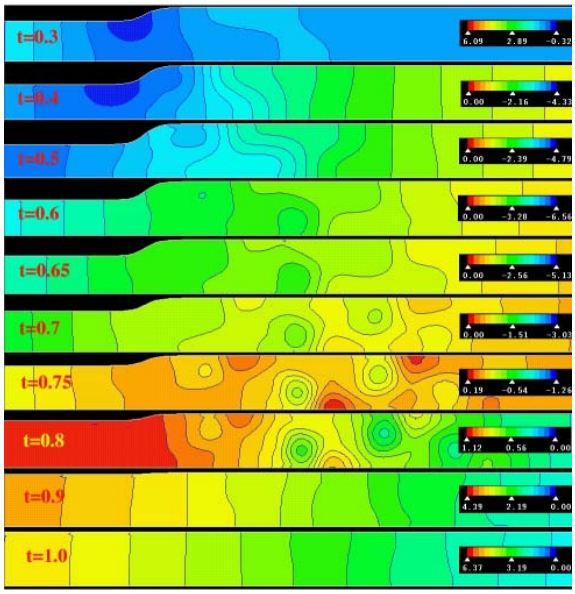

(b) Liu et al. (2000)

Fig. 11 Pressure contours at Re = 300 and $St = 0.024$ with $\varepsilon = 0.4$